Journal for ImmunoTherapy of Cancer

Depletion of conventional CD4$^+$ T cells is required for robust priming and dissemination of tumor antigen-specific CD8$^+$ T cells in the setting of anti-CD4 therapy

Delaney E Ramirez,[1,2] Christo P C Dragnev ,[2] Tyler G Searles ,[2] Nathaniel Spicer,[1] Tiffany Chen,[1] J Louise Lines,[2] Aaron R Hawkes,[2] Wilson L Davis,[2] Asmaa Mohamed,[1] Keisuke Shirai,[2,3] Joseph D Phillips,[2,4] Pamela C Rosato,[1,2] Yina H Huang,[1,2] Mary Jo Turk [1,2]

To cite: Ramirez DE, Dragnev CPC, Searles TG, *et al*. Depletion of conventional CD4$^+$ T cells is required for robust priming and dissemination of tumor antigen-specific CD8$^+$ T cells in the setting of anti-CD4 therapy. *Journal for ImmunoTherapy of Cancer* 2024;**12**:e010170. doi:10.1136/jitc-2024-010170

► Additional supplemental material is published online only. To view, please visit the journal online (https://doi.org/10.1136/jitc-2024-010170).

Accepted 15 October 2024

For numbered affiliations see end of article.

Correspondence to
Dr Mary Jo Turk;
Mary.jo.turk@dartmouth.edu

ABSTRACT

Background Overcoming immune suppression is a major barrier to eliciting potent CD8$^+$ T cell responses against cancer. Treatment with anti-CD4 monoclonal antibody is an effective means for eliminating CD4$^+$Foxp3$^+$ regulatory (Treg) cells in preclinical models and has also demonstrated efficacy in early clinical trials. However, the underlying basis for treatment efficacy, more specifically the implications of codepleting other CD4-expressing cell compartments in tumor-bearing hosts, is not well understood.

Methods Tumor-bearing mice were treated with anti-CD4 versus other therapies that preserve helper T cell function, and the priming, tissue distribution, and maintenance of tumor antigen-specific CD8 T cells were assessed. Antibody blockade and transgenic mouse models were used to determine the mechanisms of CD8 T cell priming. Single-cell RNA-sequencing (scRNAseq) was used to further characterize CD8 T cells that are primed by anti-CD4 therapy and to identify immunosuppressive CD4 T cell subsets in human melanoma following immune checkpoint blockade (ICB).

Results Comparing anti-CD4 to dual ICB therapy, we show that anti-CD4 facilitates more robust priming of TCF-1$^+$, IL-2-producing, tumor-specific CD8$^+$ T cells that disseminate to tissues and form memory. By decoupling priming from homeostatic proliferation and associated cytokines, we find that anti-CD4 functions independently of creating homeostatic space for CD8$^+$ T cells. We also show that depletion of CD4-expressing antigen-presenting cell subsets is not required for anti-CD4 efficacy. Instead, robust tumor-specific CD8$^+$ T cell priming and memory generation required the removal of total antigen-specific CD4$^+$ T cells, including both Tregs and CD4$^+$ Foxp3-negative conventional (Tconv) cells. In particular, the elimination of CD4$^+$ Tconv cells was necessary for the accumulation and maturation of conventional type-1 dendritic cells in tumor-draining LNs, which were required for CD8$^+$ T cell priming. Accordingly, anti-CD4 treatment restored CD8$^+$ T cell responses in mice cotreated with dual ICB. scRNAseq of melanoma tumors from patients who received ICB revealed the presence of Tr1 and Treg subsets, as well as CD4$^+$ Tconv subsets that lacked clear transcriptional evidence of helper differentiation.

WHAT IS ALREADY KNOWN ON THIS TOPIC

⇒ Prior studies have shown that anti-CD4 depleting monoclonal antibody therapy induces protective CD8 T cell responses against tumors in a variety of mouse models and in combination with other immunotherapy drugs. Humanized anti-CD4 has also been administered to patients with solid tumors, with promising initial results. Anti-CD4 is known to function by depleting CD4$^+$Foxp3$^+$ Tregs, which are a major barrier to antitumor immunity.

WHAT THIS STUDY ADDS

⇒ This study shows that depletion of conventional CD4+T cells is a key requirement for anti-CD4 efficacy. Depletion of total CD4+T cells uniquely induces accumulation and maturation of conventional type-1 dendritic cells (cDC1s) in tumor-draining lymph nodes, and cDC1-dependent priming of CD8 T cells that produce IL-2 and differentiate into tissue-wide memory. The CD8 T cell response induced by anti-CD4 is not dependent on the creation of homeostatic space, or on the depletion of CD4-expressing antigen-presenting cells, and is more robust than that induced by dual immune checkpoint blockade (ICB) therapy. CD4$^+$ T cell subsets with transcriptional evidence of suppressive function remain abundant in tumors of melanoma patients who underwent ICB therapy.

HOW THIS STUDY MIGHT AFFECT RESEARCH, PRACTICE OR POLICY

⇒ This study underscores the importance of targeting CD4$^+$ Tconv cells in future clinical efforts to promote systemic primary and memory CD8$^+$ T cell responses in patients with cancer.

Conclusions These findings underscore the underappreciated benefit of depleting CD4+ Tconv cells to promote systemic primary and memory CD8+ T cell responses against cancer.

BACKGROUND

Treatment with monocolonal anti-CD4 antibodies has long been used to deplete regulatory T cells (Tregs) and elicit antitumor immunity.[1–3] In contrast to Treg-depleting antibodies, such as anti-CTLA-4, anti-CD25, or anti-CCR4[4 5] antibodies against CD4 completely deplete Foxp3+ Tregs in tumors and throughout tissues.[6] Preclinical studies have shown that anti-CD4 elicits robust and persistent tumor Ag-specific CD8+ T cell responses in mouse tumor models as a monotherapy and in combination with immune checkpoint blockade (ICB).[2 7 8] Such responses appear largely independent of CD4+ T cell help.[9 10] Antibody-mediated CD4+ T cell depletion can also be achieved in humans, with a humanized defucosylated IgG1 anti-CD4 mAb affording disease stabilization and shrinkage in a small study of patients with advanced solid tumors.[11] These results highlight the potency and feasibility of CD4 depletion therapy, both preclinically and clinically. However, the underlying mechanisms of anti-CD4 efficacy remain incompletely understood.

Though the success of anti-CD4 is widely attributed to the depletion of CD4+ Foxp3+ Tregs,[2 3 12] the removal of other CD4-expressing cells may also play an important role. One potential mechanism is through the creation of homeostatic space. We and others have shown that host CD8+ T cells expand and increase expression of CD44 in mice treated with anti-CD4.[8 9] Indeed, in lymphopenic RAG knockout mice, homeostatic proliferation is known to promote CD8+ T cell activation and reactivity against tumor antigens.[13 14] Accordingly, T cell receptor (TCR) repertoire analysis in gastric cancer patients treated with anti-CD4 mAb revealed that pre-existing and new CD8+T cell clones expand in blood following anti-CD4 treatment. The degree of clonal expansion was correlated with the extent of CD4 depletion, which was speculated to depend on "space" created by CD4+ T cell removal.[15] Homeostatic proliferation is dependent on IL-7 and IL-15,[16 17] although it is unknown whether homeostatic space or associated cytokines support tumor-Ag specific CD8+ T cell priming during anti-CD4 treatment.

A second putative mechanism involves the removal of the Foxp3-negative CD4+ conventional (Tconv) cell b. Indeed, IL-10-producing CD4+T cells such as type 1 regulatory T cells (Tr1s)[18] and CCR8+CD25+Foxp3− Tconv cells,[19] both mediate tumor immune suppression. On the other hand, CD4+ Th1 cells which produce IFN-γ can clearly contribute to antitumor immunity.[20] Anti-CD4 efficiently removes all Tconv cell subsets, although it is not known if this is beneficial or detrimental for the tumor-specific CD8+ T cell response. It is also unclear whether ICB treatments that preserve CD4+ cells elicit more robust or long-lived tumor-specific CD8+ T cell responses compared with anti-CD4 therapy.

Finally, anti-CD4 may function through targeting CD4-expressing antigen-presenting cells (APCs). Indeed, CD4 is expressed by subpopulations of macrophages and plasmacytoid dendritic cells (pDCs) and by most conventional type 2 DCs (cDC2s). cDC2s are known to prime CD4+ T cell responses, and targeted depletion of Tregs in Foxp3-DTR mice promotes cDC2 migration and generation of cytotoxic CD4+ T cell responses against melanoma.[21] In tumor-bearing mice depleted of total CD4+ T cells, it is not known whether codepletion of CD4-expressing cDC2s may skew in favor of type 1 DCs (cDC1s) which promote CD8+ T cell responses.[22]

Here, we investigate the underlying mechanisms whereby anti-CD4 treatment induces CD8+ T cell responses against cancer. We compare anti-CD4 with dual ICB (anti-PD-1 + anti-CTLA-4) to define how these contexts afford different properties to de novo primed tumor Ag-specific CD8+ T cells. We also uncouple anti-CD4 efficacy from the creation of homeostatic space and the depletion of CD4-expressing APCs. Instead, we find that the removal of total CD4+ T cells—including both Tregs and Tconv cells—is critical for priming robust and persistent CD8+ T cell responses in tumor-bearing hosts. Extending relevance to human cancer, we show that CD4+ subsets with immunosuppressive characteristics are dominant in melanoma tumors from patients even following neoadjuvant ICB therapy. This work underscores the importance of depleting total CD4+ T cells in future cancer clinical trials.

RESULTS

Anti-CD4 is more potent than dual ICB at inducing tumor-specific CD8+ effector T cells that disseminate and persist as memory

We and others have shown that anti-CD4 treatment breaks CD8+ T cell tolerance to shared melanoma/melanocyte antigens in B16 tumor-bearing mice.[2 23] While primary B16 tumors are resistant to anti-CD4 treatment, mice generate systemic CD8+ T cell responses which mediate concomitant immunity against melanoma rechallenge on the opposite flank.[2] B16 is a poorly immunogenic tumor that is also resistant to anti-CTLA-4 and anti-PD-1 dual ICB therapy.[24] Compared with anti-CD4 treatment, dual ICB afforded better primary B16 tumor growth control (figure 1A,B). Thus, we sought to determine if dual ICB also induced stronger CD8+ T cell priming against a tumor-expressed antigen. Tumor-specific CD8+ T cell responses were tracked by adoptively transferring 10^4 naïve, congenically marked (Thy1.1+) TCR transgenic 'pmel' cells specific for $gp100_{25\text{-}33}$, as we have previously described.[7]

On day 12, we found that dual ICB and anti-CD4 gave rise to similar proportions of pmel cells and total CD8+ T cells in B16 tumors (figure 1C,D). However, in tumor draining lymph nodes (TDLNs), anti-CD4 induced three-fold higher proportions of pmel cells compared with dual ICB (figure 1D). Similarly, in the spleen, where essentially no pmel cells accumulated without treatment,

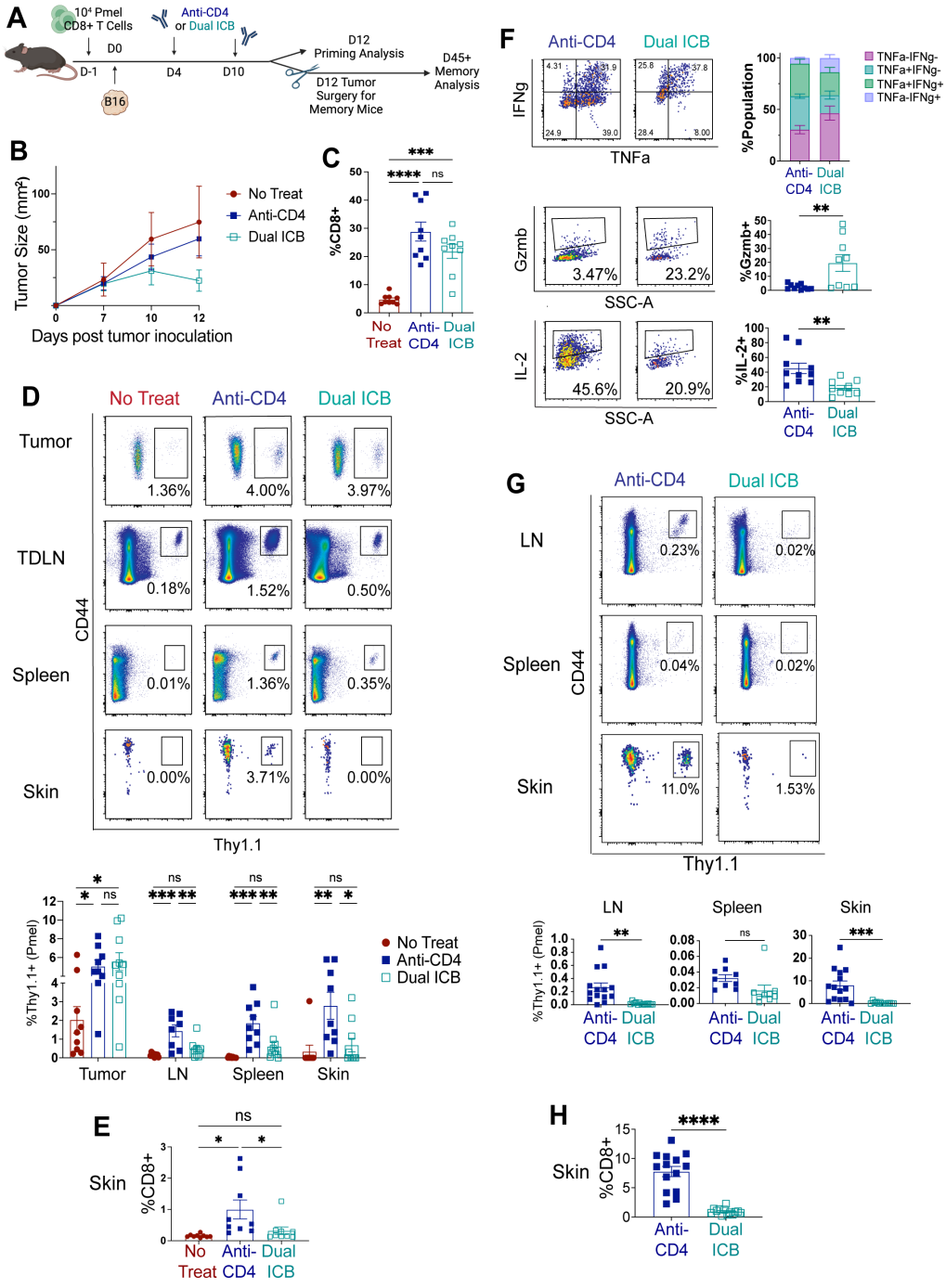

Figure 1 Priming, dissemination, and persistence of tumor Ag-specific CD8$^+$ T cells is induced by treatment with anti-CD4 but not dual ICB (anti-CTLA-4 + anti-PD-1). (A) Naïve pmel CD8+T cells were transferred into mice 1 day prior to implanting intradermal B16 tumors. Mice were untreated or treated with either anti-CD4 or anti-PD1+ anti-CTLA-4 on days 4 and 10 after tumor inoculation. Flow cytometric analysis was performed on day 12 after tumor injections. (B) Tumor growth curves. (C) Proportion of CD8$^+$ T cells in tumors on day 12, gated out of live lymphocytes. (D) Proportion of CD44^{hi} Thy1.1$^+$ pmel cells, gated out of live CD8$^+$ T cells, in the indicated tissues on day 12, compared between treatment groups. (E) Normalized (relative to anti-CD4) proportion of CD8$^+$ T cells in skin (gated on live lymphocytes) on day 12. (F) T cells from day 12 lymph nodes were restimulated for intracellular cytokine staining, and proportions of IFNγ,TNF-α, Gzmb, and IL-2-producing cells (gated on live CD8$^+$Thy1.1$^+$ pmel cells) were analyzed; gated on live CD8$^+$Thy1.1$^+$ pmel cells. (G) CD44^{hi} Thy1.1$^+$ pmel cells gated out of live CD8$^+$ T cells, across tissues, at a memory timepoint (30 days after tumor excision surgery). (H) Proportion of CD8$^+$ T cells in skin 30 days postsurgery; gated out of live CD45+lymphocytes. Each experiment was repeated at least two times with similar results and n≥4 mice per group; n.s. signifies a p>0.05. Data are pooled from two (C–F) or three (G, H) experiments. Each symbol represents an individual mouse, and flow plots depict representative mice; Bars signify the mean with error bars depicting SEM. For experiments with two groups, a paired t-test was used to determine statistical significance, and for those with more than two groups, a one-way ANOVA with multiple comparisons was used. ANOVA, analysis of variance; ICB, immune checkpoint blockade; TDLN, tumor draining lymph node; *p<0.05, **p<0.01, ***p<0.001, ****p<0.0001.

anti-CD4 induced a threefold larger proportion of pmel cells than dual ICB (figure 1D). Extending this analysis to mice-bearing MC38 tumors expressing OVA as a model tumor neoantigen, we also observed stronger priming of OT-1 $CD8^+$ T cells in TDLNs and greater dissemination to spleen with anti-CD4 as compared with dual ICB (online supplemental figure 1). Further, in the B16 model, anti-CD4 induced robust pmel (and total $CD8^+$ T cell) infiltration in the skin where cognate Ag is expressed, whereas dual ICB elicited a minimal skin response (figure 1D,E). Together, these results show that CD4 depletion drives stronger priming and dissemination of tumor Ag-specific $CD8^+$ T cells than dual ICB.

It remained possible that $CD8^+$ T cells induced by anti-CD4 were functionally inferior to those induced by dual ICB, especially due to the absence of $CD4^+$ Tconv cells which promote $CD8^+$ T cell memory.[25] Interestingly, however, anti-CD4 and dual ICB induced similar proportions of pmel cells in TDLNs that were capable of coproducing IFN-γ and TNF-α (figure 1F). Moreover, while a significantly higher proportion of pmel cells from dual ICB-treated mice produced granzyme B (figure 1F), more pmel cells from anti-CD4 treated mice produced IL-2 (figure 1F), which is associated with memory potential.[26] To assess whether $CD8^+$ T cell responses primed by dual ICB treatment could generate memory, tumors were surgically excised, and pmel responses were assessed 30 days later. We have previously shown that anti-CD4 treated mice develop melanoma-associated vitiligo which promotes resident and circulating memory T cells that afford long-term melanoma protection in skin, lungs, liver, and lymph nodes.[7 27 28] While dual ICB also induced vitiligo, the depigmentation was weaker and less widespread (online supplemental figure 2A). Moreover, in contrast to anti-CD4 treatment, pmel cells primed during dual ICB treatment largely failed to persist 30 days postsurgery (figure 1G,H), which similar to what we have previously shown in untreated tumor-excised mice.[7 29] Among polyclonal $CD44^{high}CD62L^{low}$ $CD8^+$ T cells in TDLNs, anti-CD4 induced a greater proportion of $CD103^+CD69^+$ T_{RM} cells, of which a greater proportion were also $CXCR6^+CD127^+$ (online supplemental figure 2B). Together these data demonstrate that anti-CD4 and dual ICB induce distinct responses, with the absence of $CD4^+$ T cells paradoxically promoting greater programming, dissemination, and persistence of tumor Ag-specific memory $CD8^+$ T cells.

To better understand the intrinsic differences in $CD8^+$ T cells primed by anti-CD4 versus dual ICB treatment, we also conducted single-cell RNA sequencing (scRNAseq) on endogenous Ag-experienced ($CD44^{high}$ $CD62L^{low/intermediate}$) $CD8^+$ T cells sorted from day 12 TDLNs (online supplemental figure 3), with paired TCR-sequencing to define expanded clonotypes. UMAP projection of 5204 cells sorted from combined untreated, anti-CD4, and dual-ICB treated mice resolved 6 distinct clusters (figure 2A). The largest cluster, termed "C0-MPEC" resembled memory precursor effector cells (MPECs), expressing high *Il7r* and effector transcripts including *Nkg7*, *Klrk1*, and *Klf2* (figure 2B). On the other hand, "C1-Stem-Like" had the highest levels of *Tcf7*, *Ccr7*, *Sell*, and *Jun* (figure 2B). "C2-Tpex" similarly expressed stem-associated transcripts, but also *Slamf6*, *Pdcd1*, *Ctla4* and *Lag3*, as well as *Ifng*, *Tnf*, and *Il2* (figure 2B), suggesting a progenitor exhausted state.[30] "C3-Prolif-Eff" expressed proliferation-associated genes, such as *Birc5*, *Stmn1* and *Mcm3* as well as *Gzma* and *Gzmb*, whereas "C4-Exhausted" had the highest expression of *Tox* and high *Mki67* and *Il2rb* (figure 2B). The smallest cluster, "C5-Recent-Act" had high *Tnfrsf9* (4-1BB), *Cd69*, *Il2ra*, and *Nr4a1* (figure 2B), indicative of activated T cells.[31 32] Altogether, these TDLN clusters resembled known stages of $CD8^+$ T cell activation previously described in the setting of cancer.[32]

We next compared $CD8^+$ T cell clustering and clonal expansion between the treatment groups (figure 2C). Whereas cells from untreated mice were limited to the left side of the UMAP in the C1-Stem-like, C2-Tpex, and C5-Recent-Act clusters, cells from anti-CD4 treated mice tended to populate the right of the UMAP in the C3-Prolif-Eff and C0-MPEC clusters. In contrast, cells from dual ICB mice were more intermediate in their distribution across all clusters in the UMAP, and cells from all three groups contributed to the C4-Exhausted cluster (figure 2C). Assessing the level of T cell clonal expansion between the groups, we found that untreated mice had the lowest frequency of clonotypes that had expanded and most of these were only minimally expanded (figure 2D). In contrast, anti-CD4 treatment resulted in the largest frequency of expanded clonotypes, which mainly fell within the C3-Prolif-Eff and C0-MPEC clusters (figure 2D). Dual ICB also induced expansion of clonotypes in these two clusters, with some very highly expanded clonotypes (figure 2D). Taken together, these results suggest that both anti-CD4 and dual ICB induce the proliferation and activation of effector cells and memory precursors in TDLNs, but that the response is more clonally diverse with anti-CD4 treatment.

In addition to endogenous polyclonal $CD8^+$ T cells, we also sorted pmel cells for scRNAseq (figure 2E). Comparison across the treatment groups revealed that pmel cell UMAP clustering mirrored that of polyclonal antigen-experienced $CD8^+$ T cells (figure 2E). Moreover, pseudobulk analysis of transcripts from pmel cells from untreated TDLNs revealed high stem-associated transcripts (eg, *Tcf7* and *Slamf6)*, and lower expression of effector transcripts (eg, *Gzma*, *Klf2*, *Eomes*, and *Tbx21*), whereas those from anti-CD4 treated mice had higher levels of activation and memory-associated markers including *Cxcr3*, *Icos*, *Il2*, as well as high *Fabp5* and intermediate *Tbx21* (figure 2F), which is associated with Trm formation.[33] Interestingly, compared with dual ICB treated mice, pmel cells from anti-CD4 treated mice expressed higher *Tcf7* and *Slamf6*, but lower *Gzma* (figure 2F), with *Tcf7* and *Gzma* demonstrating inverse correlation (figure 2G). Flow cytometry confirmed a twofold higher expression of TCF-1, and twofold lower

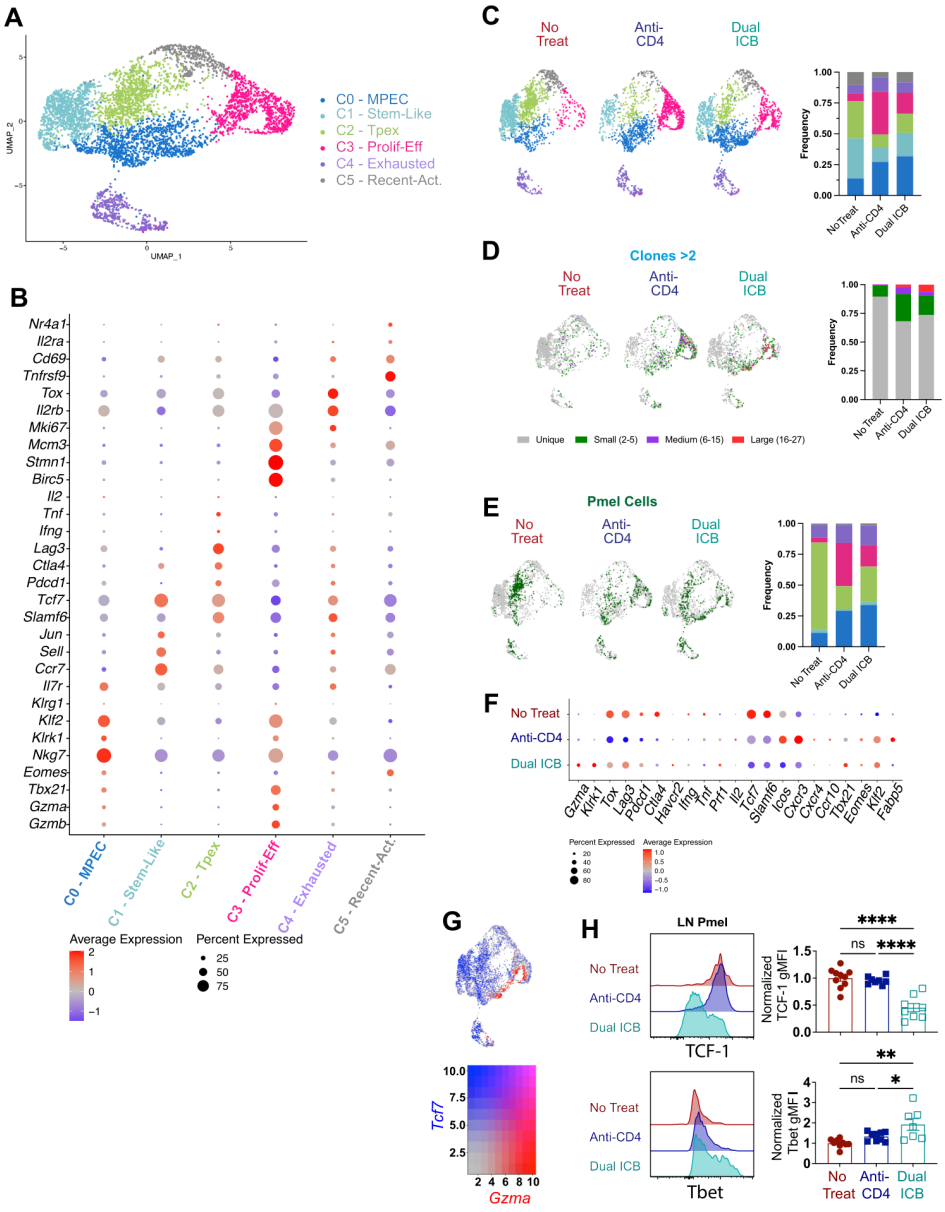

Figure 2 Compared with dual ICB, anti-CD4 induces a more diverse proliferating clonal repertoire, a reduction in progenitor-exhausted cells, and an enhancement in TCF7-expressing memory precursors. Endogenous CD44^{hi} CD62L^{lo} CD8^{+} T cells and CD44^{hi} Thy1.1^{+} pmel cells were hashtag-labeled, FACS sorted and pooled (see online supplemental figure 1) from tdLNs of five untreated, five anti-CD4-treated, and five dual ICB-treated mice on day 12. Hashtag sequences were used to identify cells from each treatment group. Gene expression was determined by single-cell RNA sequencing (scRNAseq) of 460, 325, and 460 pmel cells and 1436, 1250, and 1355 endogenous effector cells from the no treat, anti-CD4 and Dual ICB groups, respectively. Using the 10X Genomics platform. The 10X Cellranger VdJ pipeline was used to determine TCR α and β-chain CDR3 sequences. (A) UMAP plots displaying 5204 cells from the treatment groups combined, with both RNA and TCR sequencing. Each dot represents a single cell. (B) DotPlot depicting cluster-defining genes. (C) UMAP plots depicting clustering by treatment group. (D) Plots depicting clonally expanded endogenous CD8^{+} T cells, by respective treatment group, superimposed on the overall UMAP (in gray). Colors depict overall level of clonal expansion, as specified in the legend; frequency of expanded clonotypes in each of the treatment groups is shown at right. (E) UMAP plot of pmel cells (in green), by treatment group, superimposed on the overall umap; frequency of pmel cells in each of the clusters from (A) is shown, at right. (F) Pseudobulk analysis of gene expression comparing pmel cells from each of the three different treatment groups, depicting relative expression of effector and memory-associated transcripts. (G) Blended FeaturePlot illustrating the overlap between *Tcf7* and *Gzma* expression across clusters. Heatmap depicts colors that represent the extent of overlapping expression of each transcript. The colors in the upper right-hand corner depict the cells with the highest expression of each transcript that are simultaneously overlapping. Colors closer to each axis depict inverse expression of each transcript. (H) Flow cytometry analysis of Tcf1 and Tbet expression on pmel cells taken from tdLNs of anti-CD4 versus dual-ICB treated mice on day 12. Data are pooled from two independent experiments with similar results; one-way ANOVA with multiple comparisons was used to determine statistical significance, with n.s. indicating a p>0.05. For A-G, the analysis was done once. ANOVA, analysis of variance; ICB, immune checkpoint blockade; TDLN, tumor draining lymph node. *p<0.05, **p<0.01, ****p<0.0001.

expression of Tbet in pmel cells from mice treated with anti-CD4 compared with dual ICB (figure 2H), consistent with the identification of clonally expanded MPEC populations in mice treated with anti-CD4 (figure 2D). These data are consistent with the interpretation that anti-CD4 promotes stem-like memory precursors, whereas dual ICB induces more differentiated effector T cells.

Anti-CD4 efficacy does not depend on creating homeostatic space but requires the depletion of CD4+ Tconv cells

Considering the unique ability of anti-CD4 to induce tumor-specific CD8+ T cell memory, we next sought to understand its underlying mechanisms of efficacy. We have previously shown that anti-CD4 treatment induces acute homeostatic proliferation, in association with CD44 expression by host endogenous CD8+ T cells, with a return to normal CD8+ T cell proportions within 2 weeks.[9] To determine if homeostatic proliferation is required for tumor-specific CD8+ T cell priming, we instead treated with anti-CD4 beginning 14 days prior to inoculating B16 tumors and pmel cells, to afford a setting in which the window of homeostatic space had closed prior to the initiation of priming (figure 3A). Interestingly, tumor growth (figure 3B), and pmel cell proportions across TDLNs, spleen, and skin were similar in mice treated on day −14 as compared with day −1 (figure 3C), suggesting a lack of dependence on homeostatic space. As both IL-7 and IL-15 are known to drive CD8+ T cell homeostatic proliferation,[16 17] we separately used monoclonal antibodies to the IL-7 receptor (CD127) or IL-15, to neutralize the action of these cytokines during anti-CD4 treatment. However, acute blockade of neither IL-7 nor IL-15 diminished pmel cell priming (figure 3D) or subsequent memory formation (online supplemental figure 4). Taken together, these results reveal that the creation of homeostatic space is not required for anti-CD4 treatment efficacy. In contrast, antibody blockade of IL-2 receptor subunits CD122 and CD25 abrogated pmel cell priming, revealing dependence on IL-2 (figure 3E). This was notable given the role of CD4+ helper T cells as dominant producers of IL-2,[34] but consistent with our observation that pmel cells produce their own IL-2 in response to anti-CD4 treatment (figure 1F).

As the primary rationale for treating with anti-CD4 is to deplete Tregs, we next examined whether targeted elimination of Foxp3+ Tregs was sufficient to induce a systemic CD8+ T cell response of the type afforded by anti-CD4. To selectively deplete Tregs, we administered diphtheria toxin (DT) to Foxp3-DTR mice and assessed the priming of pmel cells relative to wild-type (WT) untreated and CD4-depleted mice (figure 4A; online supplemental figure 5). While targeted Foxp3+ Treg depletion resulted in better control of primary tumors (online supplemental figure 6A), similar proportions of pmel cells accumulated in tumors of Treg-depleted and CD4-depleted mice (figure 4B). Furthermore, in TDLNs, Treg and CD4 depletion led to similar proportions of pmel cells (figure 4B), indicating that, in contrast to dual ICB treatment, Treg depletion is required for robust CD8+ T cell priming. However, targeted Foxp3+ Treg depletion did not promote pmel cell accumulation in spleen or skin (figure 4B), indicating that depletion of total CD4-expressing cells is required for systemic dissemination of tumor-specific CD8+ T cell responses. Treg depletion promoted polyclonal CD8+ T cell access to skin, but the absence of pmel cells in skin underscored the Ag-irrelevant nature of this response (figure 4C). Finally, we investigated whether pmel cells primed in Treg depleted mice could persist as memory. As targeted Foxp3+ Treg depletion causes fatal autoimmunity in mice,[35] only two mice survived 1 month following tumor excision. However, surviving mice neither developed vitiligo nor sustained detectable pmel cell populations (online supplemental figure 6B). Thus, the promotion of systemic and durable CD8+ T cell responses in tumor-bearing mice required the depletion of total CD4-expressing cells.

To confirm an immunosuppressive role for Ag-specific CD4+ T cells independent of anti-CD4 treatment, we separately implanted B16 tumors in RAG knockout mice that had been reconstituted with either polyclonal WT CD4+ T cells or TCR transgenic OTII T cells (figure 4D). In the latter group, both Tregs and Tconv cells were present, but neither could engage tumor Ag. Pmel cells were cotransferred to track the CD8+ T cell response (figure 4D). Pmel cell priming in TDLNs trended to be higher in mice with Ag-irrelevant OT-II CD4+ T cells, although the difference did not reach significance (figure 4E). Importantly, however, pmel cell responses in spleen and skin (figure 4E) and the proportion of total CD8+ T cells in skin and tumor (figure 4F) were significantly higher in mice reconstituted with OT-II as compared with WT CD4+ T cells. These data support the conclusion that antigen-specific CD4+ T cells naturally suppress the generation of tumor Ag-specific CD8+ T cell responses. Interestingly, the pmel cell proportion in tumors was not enhanced by the elimination of Ag-specific CD4+ T cells, consistent with our finding that anti-CD4 has a minimal effect on primary tumor growth and a greater effect on systemic immunity (figure 1B,C). Altogether, the above results demonstrate that the induction of tumor-specific CD8+ T cell priming on anti-CD4 treatment requires the elimination of antigen-specific Tconv responses, in addition to Tregs.

Depletion of CD4+ Tconv cells is required for cDC1-mediated priming of Ag-specific CD8+ T cells in tumor-bearing mice

Prior studies have shown that targeted Foxp3+ Treg depletion facilitates increased activation of migratory type 2 conventional DCs (cDC2s) in tumor-bearing mice, thus facilitating a potent CD4-mediated response against B16 melanoma.[21] As cDC2s are known to express CD4,[36] this presented the possibility that anti-CD4 may also function, in part, by depleting cDC2s. Indeed, varying proportions of APCs, including pDCs, macrophages, and cDC2s, express CD4 (figure 5A), and staining with a distinct anti-CD4 clone revealed their efficient depletion

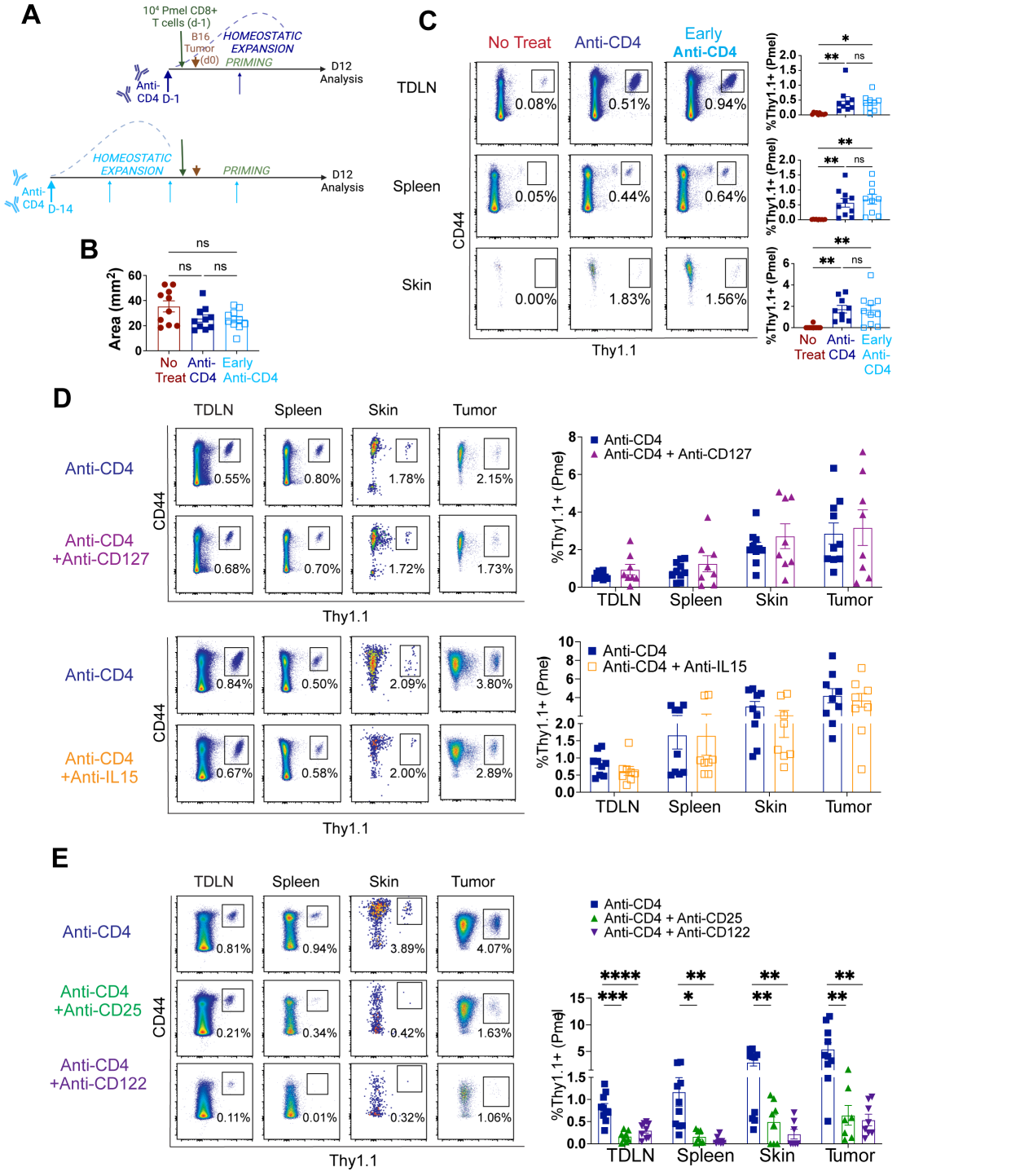

Figure 3 IL-2 is required, but homeostatic space, IL-7, and IL-15 are all dispensible, for tumor Ag specific CD8$^+$ T cell priming during anti-CD4 therapy. (A) As depicted, for B, C, mice were either left treated, or treated with anti-CD4 beginning either 14 days or 1 day(s) prior to transfer of 10^4 naïve pmel cells and B16 tumor cell inoculation on day 0. Proportion of CD44^{hi} Thy1.1$^+$ pmel cells out of live CD8$^+$ T cells was analyzed across tissues, twelve days post tumor inoculation. (B) Tumor sizes on day 12. (C) Proportions of CD44^{hi} Thy1.1$^+$ pmel cells (gated on live CD8+ T cells) were analyzed across tissues on day 12. For (D, E) Pmel cells and B16 tumors were transferred and implanted into mice and mice were treated with anti-CD4 in addition to either PBS or neutralizing antibodies against CD127 or IL-15 (D) or CD25 or CD122 (E) on days 4 and 10 after tumor inoculation. Representative flow cytometry plots of proportions of pmel Thy1.1$^+$ cells (gated out of live CD8$^+$ T cells) across tissues from each treatment group are depicted with bar graphs adjacent to them. Bar graphs show mean and SEM of data. All experiments were repeated at least twice with n≥3 mice per group; data from each panel are pooled from two independent experiments. Flow plots depict representative mice; bars represent means and error bars represent SEM. One-way ANOVA with multiple comparisons was used to determine statistical significance for experiments with more than two groups. Paired t-test was used to determine statistical significance in experiments with two groups; n.s. indicates p>0.05. ANOVA, analysis of variance; TDLN, tumor draining lymph node; *p<0.05, **p<0.01, ***p<0.001, ****p<0.0001.

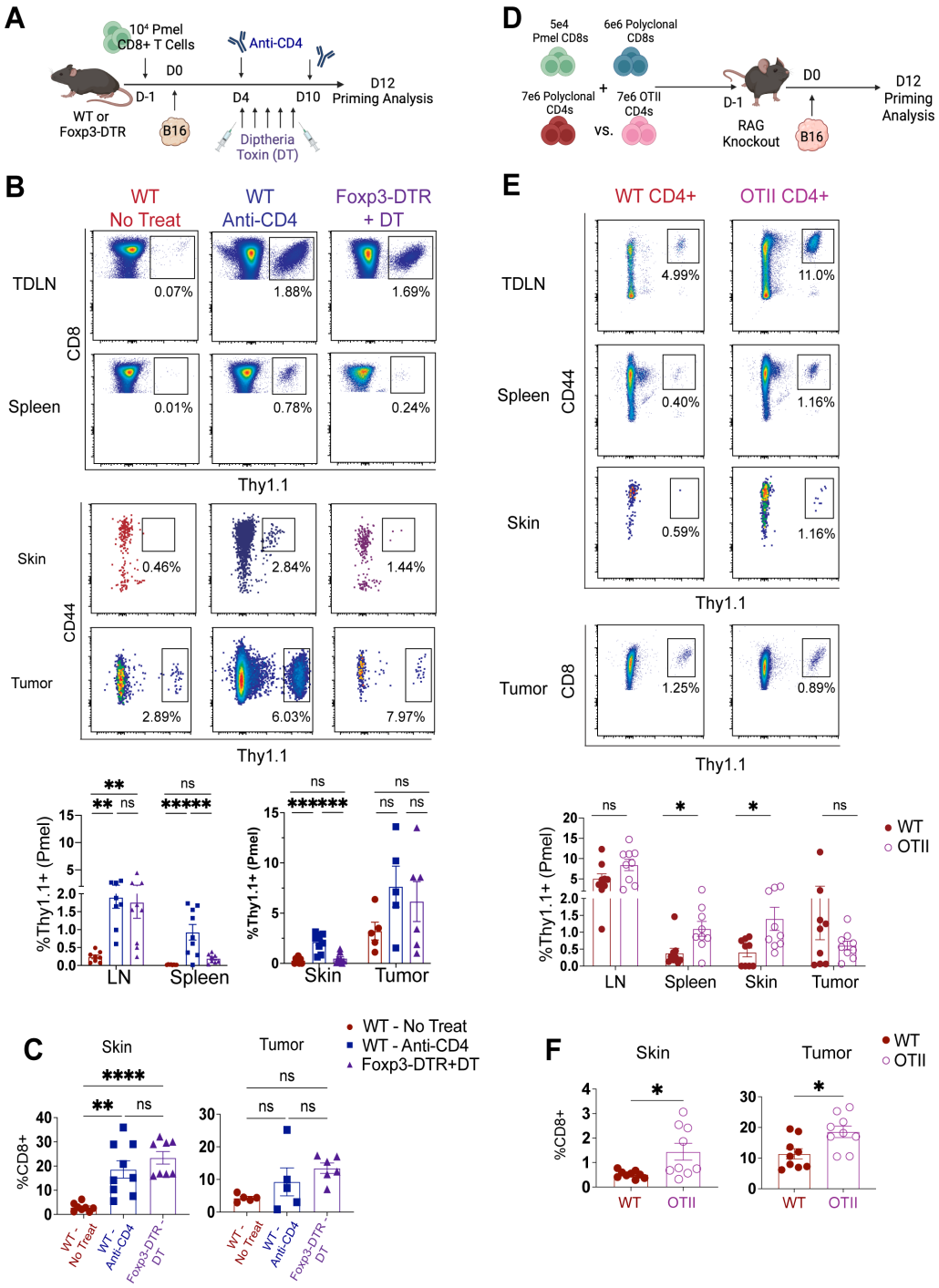

Figure 4 Removal of Ag-specific CD4$^+$ T cells is required to induce systemic CD8$^+$ T cell responses against tumor antigens. (A) Congenically marked Thy1.1$^+$ pmel cells were transferred into Foxp3-DTR and WT B6 mice 1 day prior to tumor inoculation. WT mice were either untreated or treated with anti-CD4 on days 4 and 10 after tumor inoculation. Foxp3-DTR mice were treated for five consecutive days with DT beginning on day four post tumor injection. Tissues were harvested for flow cytometry analysis on day 12 after tumor inoculation. (B) Proportion of Thy1.1$^+$ pmel cells; gated on live CD8$^+$ T cells across tissues on day 12. (C) Proportion of total CD8$^+$ T cells, gated on live CD45$^+$ lymphocytes in skin and tumor on day 12. (D) RAG knockout mice were reconstituted with polyclonal CD8$^+$ T cells and congenically marked pmel cells along with either polyclonal CD4$^+$ T cells or OTII CD4$^+$ T cells 1 day prior to tumor implantation. Tumors were left to grow for 12 days prior to analyzing pmel cell priming and dissemination by flow cytometry. (E) Proportion of CD44^{hi} Thy1.1$^+$ (TDLN, Spleen, Skin) or CD44^{hi} (tumor) pmel cells, gated on live CD8$^+$ T cells on day 12. (F) Proportion of total CD8+T cells, gated on live lymphocytes in skin and tumor on day 12. Experiments were repeated twice with n≥4 mice per group. Data are pooled from two independent experiments with similar results. Flow plots depict representative mice; bars represent means and error bars represent SEM One-way ANOVAs with multiple comparisons for experiments with three groups, and paired t-tests for experiments with two groups were used to determine statistical significance. ANOVA, analysis of variance; DT, diphtheria toxin; TDLN, tumor draining lymph node; WT, wild-type; *p<0.05, **p<0.01, ***p<0.001, ****p<0.0001.

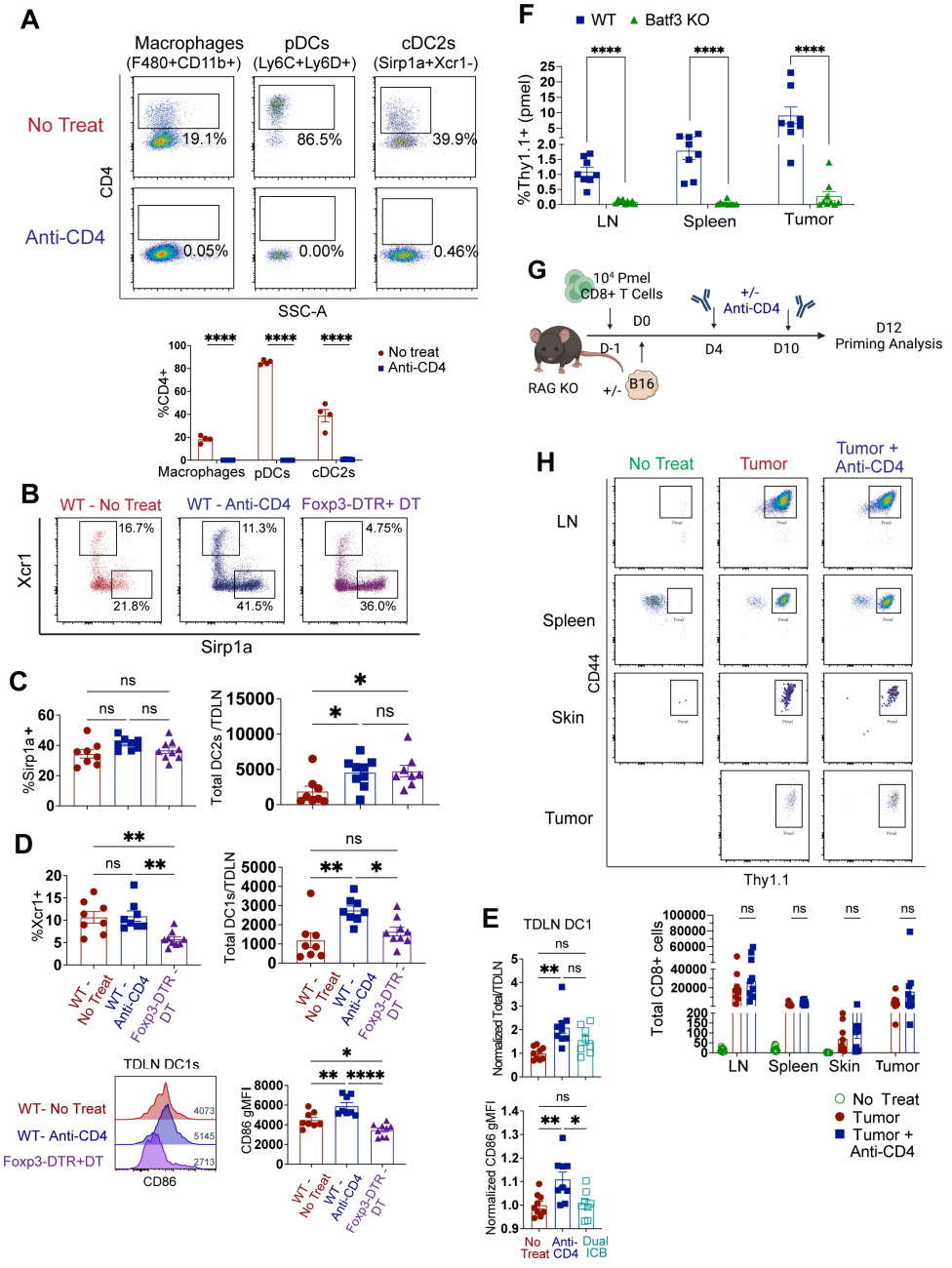

Figure 5 cDC1-dependent priming of tumor-specific CD8$^+$ T cells does not require depletion of CD4-expressing antigen-presenting cells. WT B6 mice were either untreated or treated with anti-CD4 on days 4 and 10 post intradermal B16 tumor implantation. TDLNs were digested and assessed by flow cytometry to identify various myeloid cell populations (A–D). (A) Flow plots of CD4$^+$ non-T cells in WT tdLNs on day 12. (B) Flow plots showing cDC1 and cDC2s in tdLNs on day 12. Populations are gated out of live singlets, lymphocytes, F480$^-$/CD19$^-$ cells, CD11b$^\pm$CD11c$^{+/-}$, MHCII$^+$Ly6C$^-$ cells. Xcr1$^+$Sirp1a$^-$ cells are cDC1s and Xcr1$^-$Sirp1a$^+$ cells are cDC2s. (C) Proportion of and total cDC2s per tdLN on day 12. (D) Proportion and total of cDC1s per tdLN on day 12. CD86 expression on cDC1s on day 12. (E) Mice were treated as described in figure 1A. Normalized (relative to no treat) number of cDC1s per TDLN and CD86 expression on cDC1s in TDLNs from untreated, anti-CD4 treated and dual ICB-treated mice. (F) Congenically marked pmel cells were transferred into WT B6 and Batf3 knockout mice 1 day prior to B16 implantation. Mice were treated with anti-CD4 on days 4 and 10 post tumor injection and then tissues were harvested on day 12 to assess priming by flow cytometry. Proportions CD44^{hi} Thy1.1$^+$ pmel cells out of CD8$^+$ T cells across tissues in WT and Batf3 KO mice on day 12. (G) Naïve, congenically marked pmel cells were transferred into RAG knockout mice lacking CD4$^+$ T cells. For two groups, intradermal B16 tumors were implanted 1 day later. Anti-CD4 treatment was given to deplete CD4$^+$ non-APCs 4 days after tumor implantation. (G) Pmel cells across tissues on day 12 from RAG$^{-/-}$ mice reconstituted with pmel cells only. Experiments were repeated at least two times with similar results and n≥3 mice per group. Flow plots depict representative mice; bars represent means and error bars represent SEM. One-way ANOVA with multiple comparisons was used to determine statistical significance for experiments with more than two groups. Paired t-test was used to determine statistical significance in experiments with two groups. n.s. indicates p>0.05. ANOVA, analysis of variance; cDC2s, conventional type-2 dendritic cells; ICB, immune checkpoint blockade; TDLN, tumor draining lymph node; WT, wild-type; *p<0.05, **p<0.01, ****p<0.0001.

(online supplemental figure 7, figure 5A). Unexpectedly, however, anti-CD4 treatment did not reduce total cDC2 accumulation and instead led to an increase in the total number of Sirp1a$^+$ cDC2s in TDLNs, comparable to Foxp3-DTR mice who received targeted Treg depletion (figure 5B,C). Despite this, anti-CD4 treatment promoted increased accumulation of cDC1s in TDLNs, which were more mature as evidenced by higher expression of CD86 (figure 5B,D). Importantly, elevated CD86^{hi} cDC1 populations were not observed following Foxp3-targeted Treg depletion (figure 5D), or dual ICB treatment (figure 5E), indicating that anti-CD4 was unique in promoting accumulation of CD86^{hi} cDC1s in TDLNs. Additionally, CD4 depletion induced negligible priming of pmel cells in tumor-bearing *Batf3*-knockout mice, indicating that cDC1s are required for the anti-CD4-induced CD8$^+$ T cell response (figure 5F).

While our above results collectively revealed a requirement for depleting both Treg and Tconv compartments, they did not rule out the possibility that depleting CD4$^+$ APCs also contributes to anti-CD4 effects. To test this, we employed RAG knockout mice as a model lacking both Treg and Th cells wherein anti-CD4 treatment would only deplete CD4-expressing non-T cells (figure 5G). As expected, due to the absence of Tregs and Tconv cells, B16 tumors promoted the priming and expansion of transferred naïve pmel cells in TDLNs of RAG knockout mice, as well as their accumulation in spleen and skin (figure 5H). Importantly, anti-CD4 treatment did not further enhance this response in any tissue (figure 5H). Thus, the depletion of CD4$^+$ APCs does not contribute to the cDC1-dependent priming of Ag-specific CD8+T cells in tumor-bearing mice. Rather, these data collectively support a model whereby CD4$^+$ Tconv cells naturally impair cDC1 accumulation and maturation in TDLNs, such that total CD4$^+$ T cell depletion enables cDC1-mediated priming and dissemination of tumor Ag-specific CD8$^+$ T cells.

Immunosuppressive CD4$^+$ T cell compartments persist in melanoma tumors following ICB therapy in mice and patients

Previous studies have identified Foxp3-negative Tconv subsets with immunosuppressive features in cancer, including Tr1 cells[18] and CCR8$^+$ CD25$^+$ cells.[19] We, therefore, sought the presence of these subsets in mouse and melanoma patient tumors following ICB therapy. Dual ICB led to a slight reduction in the proportion of Foxp3$^+$ Tregs in B16 tumors (figure 6A). Additionally, dual ICB reduced the proportion of recently described CCR8$^+$ CD25$^+$ Foxp3$^-$ Tconv cells in tumors (figure 6B). On the other hand, CD49b$^+$ Lag3$^+$ Tr1 cells were present in low frequencies in tumors, and these proportions were unchanged by dual ICB treatment (figure 6C). Importantly, the addition of anti-CD4 to dual ICB increased pmel proportions in TDLNs and spleens (figure 6D). Thus, suppressive CD4+T cell subsets persist in tumors of dual ICB treated mice and contribute to dampening the systemic CD8$^+$ T cell response. Prior studies in the CT-26 model have shown that anti-CD4 acts synergistically with anti-PD-1 to restrain tumor growth.[8] While we did not observe statistically improved tumor control with the addition of anti-CD4 in the B16 model, we noted that total CD4 depletion did not impair dual ICB efficacy (figure 6E,F).

To determine if CD4$^+$ T cells with immunosuppressive characteristics persist in tumors from melanoma patients following ICB treatment, we conducted scRNA seq on CD4$^+$ T cells sorted from tumors of six melanoma patients who underwent neoadjuvant ICB (anti-PD1 with or without anti-CTLA-4) (online supplemental figure 8). UMAP analysis of 4738 total cells resolved seven clusters (figure 6G). The largest cluster termed "C0-TNF/TGFB" expressed the highest levels of *IL7R, GATA3, and TNF*, but also the highest levels of *TGFB* (figure 6H). The next largest clusters "C1-Naïve-like" expressed high levels of *CCR7*, *SELL*, and *KLF2*, without evidence of effector molecule expression, and "C2-T-Undiff" did not express any notably defining transcripts. Classical immunosuppressive CD4$^+$ populations were identified, with "C3-Treg" expressing high levels of *FOXP3*, *IL2RA*, *CCR8*, *CCR4*, and *CTLA4*, and "C4-TR1" expressing canonical Tr1 markers *GZMK*, *EOMES*, *LAG3* and *IL10*, but also the highest levels of effector and exhaustion-associated transcripts *GZMA*, *IFNG*, *CXCR3, and PDCD1*. We did not observe a cluster of CCR8-expressing Foxp3- Tconv cells which may relate to its responsiveness to dual ICB treatment in the B16 model (figure 6A). Interestingly, one small cluster "C5-Tfh" expressed high levels of *ICOS*, *CXCR6*, *BCL6*, and *IL6ST*. Regardless, no cluster of CD4$^+$ T cells from ICB-treated patient tumors exemplified clear transcriptional evidence of classical helper T cell subset differentiation. In conclusion, these studies demonstrate the overwhelmingly suppressive effects of CD4$^+$ T cells that exist by default in tumor-bearing hosts, which remain intact despite ICB treatment, and which can be effectively eliminated by CD4-depletion therapy.

DISCUSSION

Promoting systemic and persistent CD8$^+$ T cell responses against cancer is critical for durable therapeutic outcomes.[37] Antibodies against CD4 have been used for two decades to deplete Foxp3$^+$ Tregs and induce robust CD8$^+$ T cell responses in various preclinical tumor models.[2 3 8] More recently, a humanized IgG1 antibody that targets CD4 has been used in patients with gastric cancer and led to tumor shrinkage and CD8$^+$ T cell clonal expansion and persistence.[11 15] Our studies here dissect the underlying mechanisms of anti-CD4 efficacy beyond its effects on Tregs. Though we and others have speculated that CD4 depletion works in part by creating homeostatic space for CD8$^+$ T cell expansion,[9 15] or by depleting CD4-expressing APCs, we rule these out as contributing factors. Instead, we show that anti-CD4 efficacy depends on eliminating CD4$^+$ Tconv cells, which suppress cDC1

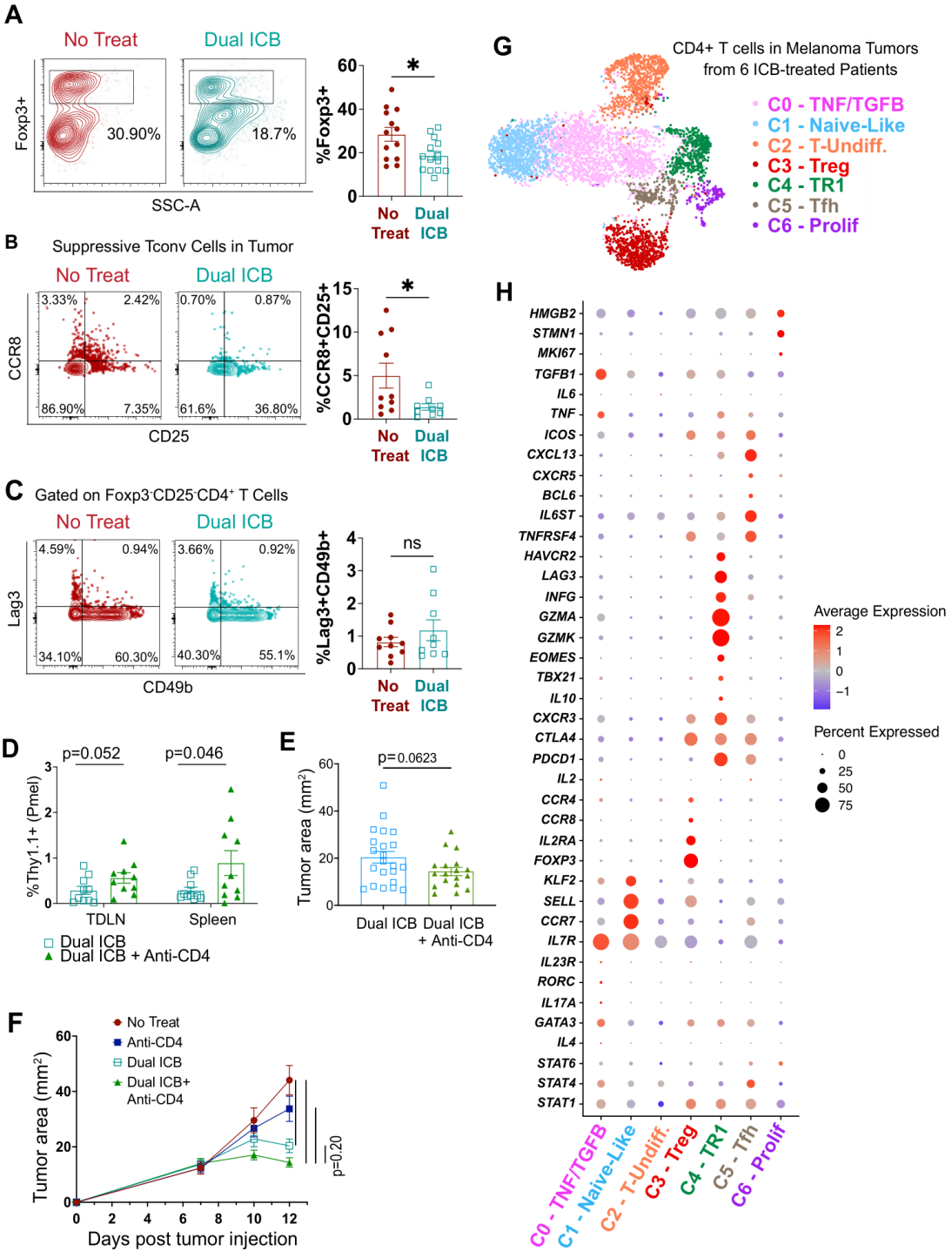

Figure 6 CD4$^+$ Tconv cells with immunosuppressive features are present in mouse and human melanoma tumors following ICB therapy. (A–C) Mice were treated as described in figure 1A. After 12 days of growth, tumors were assessed by flow cytometry. (A) Flow plots of CD4$^+$ Foxp3$^+$ T cells (B) Foxp3$^-$CD25$^-$ Lag3$^{+/-}$CD49b$^{+/-}$ CD4+ T cells. (C) Foxp3$^-$CCR8$^{+/-}$CD25$^{+/-}$ CD4$^+$ T cells. Bar graphs depict the mean and SEM. Experiments were repeated at least two times with n≥3 mice per group and similar results obtained each time. Data are pooled from 2 (B, C) or 3 (A) experiments. Paired t-tests were used to determine statistical significance. n.s. indicates p>0.05. (D–F) 10^4 naïve Pmel CD8$^+$ T cells were transferred into mice 1 day prior to implanting intradermal B16 tumors. Mice were treated with either dual ICB or dual ICB + anti-CD4 on days 4 and 10 after tumor inoculation. (D) Pmel proportions (gated out of live CD8$^+$) were assessed by flow cytometry on day 12. Bar graphs depict mean±SEM. Unpaired t-tests and Mann-Whitney U test were used to determine statistical significance. (E, F) Comparison between tumor sizes on day 12 (E), and growth curves (F) of B16 tumors in mice that were treated with dual ICB +/– anti-CD4 on days 4 and 10, as indicated. Unpaired t-test, and two-way ANOVA with multiple comparisons were used to determine statistical significance in E, F, respectively. (G) CD4$^+$ TILs were FACs sorted from six different patients and submitted for scRNA seq using the 10X genomics platform. UMAP plot of 4738 cells from all patients. Each dot represents an individual cell. (H) DotPlot of defining genes for clusters. ANOVA, analysis of variance; ICB, immune checkpoint blockade; *p<0.05.

maturation and limit CD8+ T cell priming and dissemination in tumor-bearing hosts.

Compared with dual ICB, we show that anti-CD4 promotes more robust and systemic tumor Ag-specific CD8+ T cell responses. Whereas anti-CD4 and certain isoforms of anti-CTLA-4 are known to deplete intratumoral Tregs,[3 38] anti-PD1 works by relieving CD8+ T cell exhaustion[39] and by mobilizing stem-like memory T cells[40] in tumors. However, the ability of dual ICB to induce de novo priming of tumor Ag-specific CD8+ T cells has remained incompletely understood. Prior studies have suggested that newly primed T cells are dispensable for the antitumor effects of dual ICB, as treatment to inhibit T cell migration does not impair efficacy.[41] Our finding that dual ICB promoted better control of tumors than anti-CD4 further suggests that tumor control and de novo CD8+ T cell priming occur independently. Nonetheless, a stronger systemic response is recognized as a key component of immunotherapy responses.[37] We show that such responses are uniquely achieved by anti-CD4 treatment, against both a shared self/tumor specific Ag, and a model tumor neoantigen. Notably, anti-CD4 resulted in the development of much stronger autoimmune vitiligo than dual ICB, consistent with its superior ability to break CD8+ T cell tolerance in melanoma tumor-bearing mice.

Our scRNAseq analysis shows that anti-CD4 promotes a robustly proliferating primary effector CD8+ T cell response without compromising memory T cell features. Though both anti-CD4 and dual ICB induced a CD8+ T cell response that was distinct from that of untreated tumor-bearing mice, the Ag-specific response induced by anti-CD4 appeared more stem-like. We previously found that anti-CD4 generates a persisting population of resident memory CD8+ T cells, as well as memory T cells that resemble stem-like memory.[28 42] Interestingly, at an early time point, we found that a stem-like population was most prevalent in TDLNs of untreated mice. It is plausible that anti-CD4 treatment promotes greater expansion and differentiation of PD-1 low stem-like cells, whereas dual ICB may clonally expand progenitor-exhausted T cells, which express higher levels of CTLA-4 and PD-1, and are known to differentiate into exhausted progeny.[43] We find that anti-CD4 generated pmel cells that also express high *Tcf7*/TCF1 and intermediate *Tbx21*/Tbet, the latter of which promotes the establishment of CD8+ Trm in the skin.[33] Of note, memory formation in anti-CD4 treated mice could additionally relate to host-conditioning effects of CD4 T cell depletion in tissues, such as the depletion of Tregs localized within skin, although this requires further study.

While prior studies have alluded to the creation of homeostatic space as an underlying mechanism of anti-CD4 efficacy, results from our experiments indicate otherwise. Early anti-CD4 treatment—to offset the windows of T cell priming and homeostatic CD8+ T cell proliferation—did not diminish the response, nor did the blockade of IL-7 or IL-15. We also showed that CD8+ T cell responses to tumor are efficiently primed in RAG knockout mice reconstituted with OT-II cells which fill T cell space without allowing an antigen-specific CD4+ T cell response. These three studies together argue against homeostatic space as a mechanism of action. In contrast to IL-7 and IL-15, our findings indicate a requirement for IL-2, even as CD4+ Tconv cells are the dominant producers of IL-2.[34] Moreover, our findings suggest that anti-CD4 treatment enables CD8+ T cells to produce their own IL-2, which could drive the rapidly proliferating population observed in our scRNAseq analysis. Interestingly, in acute lymphocytic choriomeningitis virus infection, autocrine IL-2 was only found in MPECs and not SLECs.[26] These results highlight a seemingly paradoxical mechanism by which depletion of CD4+ T cells promotes CD8 T cell memory.

While efficient Treg depletion was the original rationale for employing anti-CD4 therapy for cancer, here we establish that CD4+ Tconv codepletion is also an essential mechanism. We find that targeted Treg depletion results in priming of CD8+ T cell responses in TDLNs, but it is insufficient to induce systemic responses in spleen and skin that are achieved by total CD4+ T cell depletion. Whereas Tregs have been shown to inhibit cDC1 maturation,[44] we found that total CD4+ T cell depletion increased numbers of CD86hi cDC1s in TDLNs to a greater extent than Treg depletion alone. This, together with our finding that cDC1s are required for CD8+ T cell priming in CD4-depleted mice, suggests that CD4+ Tconv cells restrain the function of tumor Ag cross-presenting cDC1s. Of note, during growth of highly immunogenic methylcholanthrene-induced tumors, CD4+ T cells have been shown to naturally license cDC1s to prime CD8 T cells.[45] Thus, a caveat to our work is that CD4+ Tconv cell function likely varies across tumor models. Thus, future studies are needed to identify immunosuppressive Tconv subsets and their mechanisms for restraining DC function.

Indeed, our findings here provide a counterpoint to a large body of work illustrating the helpful functions of CD4+ Tconv cells in promoting CD8+ T cell responses. While properly primed CD4+ Th cells can undoubtedly enhance cancer immunotherapy and even directly reject tumors in the setting of adoptive cell therapy,[46] our work here highlights the natural tendency of Tconv cells to oppose CD8 T cell priming in tumor-bearing hosts. This is an important consideration as the field considers combining anti-CD4 with ICB treatment for patients. Recent studies have shown that Th1-like CD4+ T cells differentiate the responses of patients who received anti-CTLA-4 and anti-PD-1 and those treated only with anti-PD-1.[47] Anti-CTLA-4 treatment has also been associated with an increase in intratumoral ICOS+ CD4+ Teff cells in mice and melanoma patients.[48] In our analysis of patient tumors, a CD4+ Tconv cluster with the strongest transcriptional evidence of Th1 differentiation expressed some ICOS but was also high for canonical Tr1 markers and features of exhaustion, as seen in other studies.[49] Future work will be needed to understand if dual ICB-induced

Tconv subsets function in an immune stimulatory or suppressive capacity, to determine if anti-CD4 cotreatment is warranted.

In summary, our studies challenge the premise that anti-CD4 functions merely by depleting Tregs and reveal the importance of codepleting Tconv cells. We show that the depletion of putative "helper" T cells paradoxically improves the function and stemness of tumor Ag-specific $CD8^+$ T cells and facilitates memory generation. Importantly, the generation of systemic responses and $CD8^+$ T cell memory is a unique capability of anti-CD4 treatment, which is not achieved by Treg depletion or by dual ICB therapy. Humanized Anti-CD4 monoclonal antibodies have been shown to effectively deplete CD4+T cells in patients, with only rare reports of serious adverse events, that subsequently resolved.[11 35] As antibodies for selectively depleting $Foxp3^+$ Tregs remain elusive from a technical perspective, and potentially dangerous from an autoimmune perspective, anti-CD4 should be pursued as a viable alternative in future clinical studies.

MATERIALS AND METHODS

Mouse models

Male and female C57BL/6 mice were purchased from Charles River Laboratory and used at 7–12 weeks of age. Pmel Thy1.1 mice (strain #005023) were purchased from The Jackson Laboratory and bred in-house. All mice were housed and used in accordance with Dartmouth's Institutional Animal Care and Use Committee policies (IACUC Protocol #00002039). Foxp3-DTR (#016958), *Rag1* knockout (#002216), and *Batf3* knockout mice (#013755) were purchased from Jackson Laboratories and bred in-house. OTI (#003831) and OTII mice (#004194) were purchased from The Jackson Laboratory and bred in house to CD45.1 (#002014) and Thy1.1 mice (#000406), respectively, which were also purchased from The Jackson Laboratory. Dartmouth College's Comparative Medicine and Research facility ensured that all animals were maintained in a pathogen-free environment. Mice were kept in a controlled temperature environment with regular light and dark cycles in isolator caging units. Mice exhibiting rapid weight loss or tumor sizes above 10 mm were euthanized.

Tumor cell growth and inoculation

The B16-F10 melanoma tumor cell line was a gift from Allan Houghton at Memorial Sloan Kettering Cancer Center, and originally from Isiah Fidler at the MD Anderson Cancer Center. Tumor cells were passaged 10 times in vivo to ensure reproducible intradermal growth. For each experiment, a fresh vial of tumor cells was thawed and grown for 5 days in RPMI-1640 containing 7.5% heat-inactivated fetal bovine serum (FBS). To generate tumors, cells were harvested using trypsin, and 2×10^5 live cells were injected into the dermis. For studies to evaluate long-term memory, intradermal tumor excision surgery was performed on day 12, and wounds were closed with sterile surgical clips. MC38 tumors transduced with OVA via pCigar-OVA retroviral vector were a gift from Edward Usherwood at Dartmouth and were grown in DMEM containing 10% heat-inactivated FBS. Cells were harvested using trypsin and 6×10^5 cells were injected intradermally.

T cell isolation and adoptive transfer

A naïve $CD8^+$ T cell Iiolation kit (STEMCELL Technologies, cat #19858) was used to isolate pmel cells from LNs and spleens of naïve pmel mice. CD8 expression (anti-CD8-PE-Dazzle, clone 53-6.7), low CD44 expression (anti-CD33-FITC or APC, clone IM7), and the congenic marker Thy1.1 (anti-Thy1.1-APC-Cy7, clone OX-7) were used to confirm purity of naïve pmel cells by flow cytometry. 10^4 pmel cells were injected retro-orbitally 1 day prior to B16 tumor cell inoculation in either WT, Foxp3-DTR, or RAG knockout mice, as denoted in figure legends.

For experiments involving WT versus OTII $CD4^+$ T cell reconstitution in RAG knockout mice, biotin positive selection kits (STEMCELL #17655) were used to isolate total $CD4^+$ T cells from naïve C57BL/6 or OTII donor mice and total T cell (STEMCELL #19851) or CD8+T cell (STEMCELL #19853) isolation kits were used to isolate total CD8 T cells from naïve C57BL/6 donor mice. RAG−/− mice were each transferred with 7×10^6 naïve $CD4^+$ T cells (either WT or OT-II), 6×10^6 WT naive $CD8^+$ T cells to fill space, and 5×10^5 sentinel pmel cells. B16 tumors were inoculated 1 day later, and pmel responses were assessed after 12 days of tumor growth.

In vivo antibody and DT treatments

Treatments were assigned to each cage prior to beginning the experiment to ensure randomization of groups and minimize confounding variables. Blinding of experimental groups was not done during any part of the experiment or analysis. Rat IgG2b monoclonal anti-CD4 antibody clone GK1.5 was purchased from ATCC and grown in-house in a bioreactor using chemically defined serum-free medium. Hybridoma supernatant batches were filtered and tested in vivo for efficient depletion of $CD4^+$ cells. Mice were dosed with 200 µg GK1.5 intraperitoneally on days 4 and 10 relative to tumor implantation. Anti-PD1 (clone: RMP1-14) and anti-CTLA4 (clone: 9H10) were purchased from BioXCell and administered at 200 µg per dose, also on days 4 and 10 after tumor implantation. DT was purchased from Sigma Aldrich (#D0564) and prepared fresh in sterile PBS at 5 µg/mL. Mice were given 1 µg DT i.p, daily, on days 4–9 after tumor inoculation. Anti-IL15 (clone: AIO.3), anti-CD127 (clone: A7R34), anti-CD122 (clone: TM-Beta 1), and anti-CD25 (clone: PC-61.5.3) were ezch purchased from BioXCell. Mice were injected intraperitoneally on days 4 and 10 post tumor injection with 100 µg of anti-IL15, 300 µg of anti-CD127, 200 µg of anti-CD122 or 200 µg of anti-CD25.

Tissue harvest and processing

Mice were euthanized with CO_2 according to NIH ARAC Guidelines for Euthanasia of Rodents Using Carbon Dioxide. Spleens and lymph nodes were harvested and smashed through 40 µm filters. Red blood cell (RBC) lysis buffer (Biolegend, #420302) was used to remove RBCs from spleens prior to staining. If staining for myeloid cells from LNs or spleens, tissues were minced and then digested in collagenase IV (400 units/mL) (Worthington, LS004189) in HBSS containing Ca/Mg (Corning, #21-020-CV) for 30 min at 37°C, and then filtered prior to staining. Skin surrounding the tumor area was harvested and fat was removed prior to mincing and digesting in collagenase IV (930 units/mL) in RPMI with 5% heat-inactivated FBS, calcium (1 mM, Hyclone #SH30289.01) and magnesium (1 mM, Ambion #AM9530G), for 30 min at 37°C. Following digestion, skins were blended in gentle MACs Dissociators (Miltenyi, #130-093-25), filtered and washed in 1X PBS twice prior to staining in 96-well u-bottom plates. Tumors were harvested, minced, and digested in collagenase IV (725 units/mL in HBSS with Ca/Mg (Corning, #21-020-CV)) for 45 min at 37°C. Following digestion, tumors were filtered through 40 µm mesh and then plated for antibody staining.

Flow cytometry

Cells were suspended in flow buffer (PBS+2 mM EDTA+0.2% BSA) in 96-well u-bottom plates for staining. Live/Dead Fixable Blue (ThermoFisher, #L34962) was stained in PBS on ice for 10 min in the dark, and surface antibody stains (see online supplemental table S2) proceeded on ice for 20 min. Intracellular antibody-mediated (see online supplemental figure 8) staining was done using the True Nuclear Fixation Kit (Biolegend, #424401). Transcription factors and cytokines were stained in the dark at room temperature for 45 min.

For intracellular cytokine staining, cells were incubated with activation cocktail containing PMA-Ionomycin in the presence of Brefeldin A (1:500, Biolegend, #423303) at 37°C+5% CO_2 for 5 hours. Activation cocktail was prepared in RPMI containing 10% heat inactivated FBS, 2-ME (Sigma, #M3148), HEPES (#25-060 Cl), non-essential amino acids (Cellgro, #25-025 Cl), and sodium pyruvate (#25-000 Cl). Unstimulated cells were incubated with protein transport inhibitor containing Brefeldin A (ThermoFisher #00-4980-03) without PMA/Ionomycin. Cells were washed and stained with surface antibodies (see online supplemental figure 8) in the presence of protein transport inhibitor, then fixed, permeabilized, and stained for antibodies against cytokines. For flow cytometry analysis, FlowJo Software (V.10.8.1), was used. Phenotype analysis was done on populations with a minimum of 50 cells.

Mouse scRNAseq

For mouse $CD8^+$ T cell scRNAseq, TDLNs were harvested and pooled from three groups of B16 tumor-bearing mice (n=5 per group) on day 12 that had received either no treatment, anti-CD4, or dual ICB (anti-CTLA-4 and anti-PD-1) therapy. LNs were processed as described for flow cytometry. Antibodies against CD8 (PE-Dazzle, Clone 53.6-7), CD44 (FITC, Clone IM7), CD62L (AlexaFluor700, Clone MEL-14), Thy1.1 (APC-Cy7, OX-7) and hashtags were all used to stain cells in PBS containing 2% FBS. After staining, TDLNs from each group were stained with hashtags, which were used for later scRNA seq analysis to distinguish cells from each treatment group. Populations of antigen experienced, open-repertoire CD8+T cells ($CD8^+$ $CD44^{hi}$ $CD62L^{lo}$) and pmel T cells ($CD8^+$ $CD44^{hi}$ $Thy1.1^+$) were sorted on a SONY SH800 cell sorter. 2500 pmel cells and 7,500 $CD44^{hi}$ $CD62L^{lo}$ cells from each group were sorted and loaded in 33.8 µL onto a single lane of a Single Cell A chip (10X Genomics). Cells were processed on a Chromium instrument (10X Genomics). Amplified cDNA and TCR-specific libraries were prepared following the standard 10X procedure to generate libraries for Illumina sequencing. Samples were uniquely barcoded, pooled according to treatment group, and sequenced across multiple Illumina NextSeq500High Output runs to generate 50,000 and 5000 reads/cell for gene expression and TCR libraries, respectively. Paired end sequencing was performed using 26 cycles for read 1 to decode the 16 bp cell barcode and 10 bp UMI sequences, and 98 cycles for read 2 corresponding to the transcript sequence. Raw sequencing data were processed through the Cell Ranger V.3.0 pipeline (10X Genomics) using the mouse reference genome mm10 to generate gene expression matrices for single-cell 5' RNA-seq data and, in some instances, fully reconstructed, paired TRA/TRB sequences. Libraries underwent quality control by Fragment Analyzer and Qubit (ThermoFisher) to determine size distribution and the quantity of the libraries prepared. Raw and analyzed data are publicly available at NIH GEO.[50]

Mouse single-cell RNAseq and TCRseq analysis

As previously published,[51] the "Seurat V.4.3.0.1" R package was applied to filter out doublets and low-quality cells, normalize gene expression profiles, and cluster cells. Cells with gene expression levels above 0 for *Cd79a* and *Cd68*, and above 3 for *Cst3* were filtered out. Cells expressing >10% mitochondrial gene counts, expressing less than 200 or greater than 6000 genes, and expressing over 40,000 transcripts per cell were discarded using the subset function. The NormalizeData function was applied to normalize, and log transformed the raw counts for each cell based on the library size. Clustering of cells was performed using Seurat V.4.0 pipeline. For TCR analysis, the 10X Cellranger VdJ pipeline was used to determine each TCR α-chain and β-chain CDR3 sequence for a corresponding cell. Cells without productive TCRs were filtered out. After combining RNA and TCR sequenced cells, the data were rescaled and normalized.

Patient tumor acquisition, processing, and CD4+ T cell sorting

Types of immunotherapy and timing of surgery varied among the patients (online supplemental figure 8).

On the day of surgery, fresh tumor specimens were obtained from the operating room, weighed, placed in collagenase digestion media, and digested in a rotating rack in a 37°C for 30 min. Reactions were stopped by filling the digestion tubes with ice cold FACS sorting buffer. Samples were smashed passed through a 70 µm filter, washed in cold buffer, spun at 625 g for 8 min, and resuspended in FACS buffer.

Human CD4+ T cell isolation and scRNA sequencing

Processed human single-cell suspensions were stained with anti-CD4 and anti-CD45 fluorescent mAbs (see online supplemental table S2) for 30 min. Samples are then washed and resuspended in FACS buffer containing DAPI live dead stain. Approximately 10,000 live CD4+T cells were sorted from each tumor specimen using a Sony SH800 Cell Sorter. Sorted cells were loaded into a 10X Genomics Chip K following their protocol for 5' sequencing. Cells were processed on a Chromium instrument (10X Genomics). Amplified cDNA libraries were prepared following the standard 10X procedure to generate libraries for Illumina sequencing. Samples sequenced across multiple Illumina NextSeq500High Output runs to generate 50,000 reads/cell for gene expression.

Human scRNA seq data analysis

As with our processing for mouse CD8+T cells, the "Seurat V.4.3.0.1" R package was applied to filter out low-quality cells, normalize gene expression profiles, and cluster cells. Cells expressing >15% mitochondrial gene counts, expressing fewer than 200 or greater 3500 genes, and expressing over 12 500 transcripts per cell were discarded using the subset function and the scTransform function was applied to normalize the raw counts for each cell based on the library size. Clustering of cells was performed using Seurat V.4.0 pipeline and resolution was set based on differentially expressed genes.

Statistical analysis

GraphPad Prism V.9 software (V.9.1.2) was used for statistical analysis (GraphPad Software). Gaussian distribution of the data was assessed using the D'Agostino & Pearson test and the Shapiro-Wilk test. Normally distributed data were analyzed using an unpaired, two-sided t-test for samples with two groups or a one-way analysis of variance tests to compare more than two groups. When data were not normally distributed, the Mann-Whitney U test was used to compare samples in two groups, and the Kruskal-Wallis test was used to compare samples among more than two groups. P values were considered statistically significant when they were below 0.05.

Author affiliations
[1]Department of Microbiology and Immunology, Dartmouth College Geisel School of Medicine, Lebanon, New Hampshire, USA
[2]Dartmouth Cancer Center, Dartmouth College Geisel School of Medicine, Lebanon, New Hampshire, USA
[3]Department of Medicine, Dartmouth Health, Lebanon, New Hampshire, USA
[4]Department of Surgery, Dartmouth Health, Lebanon, New Hampshire, USA

Acknowledgements The authors thank Shawn C. Musial, Nikhil Khatwani, Cameron Messier, Steve Fiering, Fred Kolling, Melanie C. Peck, Chen-Yu Wang Sr., and Ibrahim Ozgenc for their thoughtful input, and Alexander N. Nemeth for technical assistance. Figure illustrations and graphical abstract were created in BioRender.com

Contributors DR, CPCD, TS, MJT, PR and YH contributed to conception and design; AOM, JP, and KS provided study materials or patients; DR, MJT, CPCD, TS, NS, TC, JL, AH and WD collected and assembled data; DR, CPCD, TS, NS, TC, PR, YH and MJT analyzed and interpreted data; and all authors contributed to manuscript writing and gave final approval. MJT is the guarantor.

Funding NIH T32 AI007363 to DR, NIH R01CA254042 to YH and MJT, NIH R01CA271553 to YH, NIH R01CA22502 to MJT, NIH CA269455-01A1 to PR, and the Knights of the York Cross of Honour and O. Ross McIntyre, M.D. Endowment to MJT. Core resource support was provided by the Dartmouth Cancer Center Immune Monitoring Flow Core and Genomics Core Facility and P30 CA023108.

Competing interests None declared.

Patient consent for publication Not applicable.

Ethics approval All human studies were performed with approval from the Committee for the Protection of Human Subjects at Dartmouth Health (study #D16002). Institutional review board-approved written, informed consent was obtained from patients with melanoma to use residual surgical tumor specimens, obtained during standard-of-care surgery, for research.

Provenance and peer review Not commissioned; externally peer reviewed.

Data availability statement Data are available in a public, open access repository. Data are available on reasonable request. Mouse scRNAseq data are publicly available in the NIH GEO database (https://www.ncbi.nlm.nih.gov/geo/). Deidentified human scRNAseq data are available through controlled access by the NIH dbGAP (https://www.ncbi.nlm.nih.gov/gap/). All other data and materials are available on reasonable request to the corresponding author (mary.jo.turk@dartmouth.edu).

ORCID iDs
Christo P C Dragnev http://orcid.org/0009-0003-7877-8058
Tyler G Searles http://orcid.org/0000-0003-3146-4812
Mary Jo Turk http://orcid.org/0000-0002-9612-8329

REFERENCES

1 Nagai H, Horikawa T, Oka M, *et al*. Elimination of CD4+ T Cells Enhances Anti-Tumor Effect of Locally Secreted Interleukin-12 on B16 Mouse Melanoma and Induces Vitiligo-Like Coat Color Alteration. *J Invest Dermatol* 2000;115:1059–64.
2 Turk MJ, Guevara-Patiño JA, Rizzuto GA, *et al*. Concomitant tumor immunity to a poorly immunogenic melanoma is prevented by regulatory T cells. *J Exp Med* 2004;200:771–82.
3 Yu P, Lee Y, Liu W, *et al*. Intratumor depletion of CD4+ cells unmasks tumor immunogenicity leading to the rejection of late-stage tumors. *J Exp Med* 2005;201:779–91.

4 Sugiyama D, Nishikawa H, Maeda Y, *et al*. Anti-CCR4 mAb selectively depletes effector-type FoxP3+CD4+ regulatory T cells, evoking antitumor immune responses in humans. *Proc Natl Acad Sci U S A* 2013;110:17945–50.
5 Rech AJ, Mick R, Martin S, *et al*. CD25 blockade depletes and selectively reprograms regulatory T cells in concert with immunotherapy in cancer patients. *Sci Transl Med* 2012;4:134ra62.
6 Rice JC, Bucy RP. Differences in the degree of depletion, rate of recovery, and the preferential elimination of naive CD4+ T cells by anti-CD4 monoclonal antibody (GK1.5) in young and aged mice. *J Immunol* 1995;154:6644–54.
7 Byrne KT, Côté AL, Zhang P, *et al*. Autoimmune melanocyte destruction is required for robust CD8+ memory T cell responses to mouse melanoma. *J Clin Invest* 2011;121:1797–809.
8 Ueha S, Yokochi S, Ishiwata Y, *et al*. Robust Antitumor Effects of Combined Anti–CD4-Depleting Antibody and Anti–PD-1/PD-L1 Immune Checkpoint Antibody Treatment in Mice. *Cancer Immunol Res* 2015;3:631–40.
9 Côté AL, Byrne KT, Steinberg SM, *et al*. Protective CD8 memory T cell responses to mouse melanoma are generated in the absence of CD4 T cell help. *PLoS One* 2011;6:e26491.
10 Medler TR, Kramer G, Bambina S, *et al*. Tumor resident memory CD8 T cells and concomitant tumor immunity develop independently of CD4 help. *Sci Rep* 2023;13:6277.
11 Shitara K, Ueha S, Shichino S, *et al*. First-in-human phase 1 study of IT1208, a defucosylated humanized anti-CD4 depleting antibody, in patients with advanced solid tumors. *J Immunother Cancer* 2019;7:195.
12 Palmeri JR, Lax BM, Peters JM, *et al*. CD8+ T cell priming that is required for curative intratumorally anchored anti-4-1BB immunotherapy is constrained by Tregs. *Nat Commun* 2024;15:1900.
13 Brown IE, Blank C, Kline J, *et al*. Homeostatic proliferation as an isolated variable reverses CD8+ T cell anergy and promotes tumor rejection. *J Immunol* 2006;177:4521–9.
14 Kline J, Zhang L, Battaglia L, *et al*. Cellular and molecular requirements for rejection of B16 melanoma in the setting of regulatory T cell depletion and homeostatic proliferation. *J Immunol* 2012;188:2630–42.
15 Aoki H, Ueha S, Shichino S, *et al*. Transient Depletion of $CD4^+$ Cells Induces Remodeling of the TCR Repertoire in Gastrointestinal Cancer. *Cancer Immunol Res* 2021;9:624–36.
16 Sandau MM, Winstead CJ, Jameson SC. IL-15 is required for sustained lymphopenia-driven proliferation and accumulation of CD8 T cells. *J Immunol* 2007;179:120–5.
17 Tan JT, Ernst B, Kieper WC, *et al*. Interleukin (IL)-15 and IL-7 jointly regulate homeostatic proliferation of memory phenotype CD8+ cells but are not required for memory phenotype CD4+ cells. *J Exp Med* 2002;195:1523–32.
18 Bergmann C, Strauss L, Wang Y, *et al*. T regulatory type 1 cells in squamous cell carcinoma of the head and neck: mechanisms of suppression and expansion in advanced disease. *Clin Cancer Res* 2008;14:3706–15.
19 Whiteside SK, Grant FM, Alvisi G, *et al*. Acquisition of suppressive function by conventional T cells limits antitumor immunity upon T_{reg} depletion. *Sci Immunol* 2023;8:eabo5558.
20 Poncette L, Bluhm J, Blankenstein T. The role of CD4 T cells in rejection of solid tumors. *Curr Opin Immunol* 2022;74:18–24.
21 Binnewies M, Mujal AM, Pollack JL, *et al*. Unleashing Type-2 Dendritic Cells to Drive Protective Antitumor $CD4^+$ T Cell Immunity. *Cell* 2019;177:556–71.
22 Hildner K, Edelson BT, Purtha WE, *et al*. Batf3 deficiency reveals a critical role for CD8alpha+ dendritic cells in cytotoxic T cell immunity. *Science* 2008;322:1097–100.
23 Aoki H, Ueha S, Shichino S, *et al*. TCR Repertoire Analysis Reveals Mobilization of Novel $CD8^+$ T Cell Clones Into the Cancer-Immunity Cycle Following Anti-CD4 Antibody Administration. *Front Immunol* 2018;9:3185.
24 van Elsas A, Hurwitz AA, Allison JP. Combination immunotherapy of B16 melanoma using anti-cytotoxic T lymphocyte-associated antigen 4 (CTLA-4) and granulocyte/macrophage colony-stimulating factor (GM-CSF)-producing vaccines induces rejection of subcutaneous and metastatic tumors accompanied by autoimmune depigmentation. *J Exp Med* 1999;190:355–66.
25 Shedlock DJ, Shen H. Requirement for CD4 T cell help in generating functional CD8 T cell memory. *Science* 2003;300:337–9.
26 Sarkar S, Kalia V, Haining WN, *et al*. Functional and genomic profiling of effector CD8 T cell subsets with distinct memory fates. *J Exp Med* 2008;205:625–40.
27 Malik BT, Byrne KT, Vella JL, *et al*. Resident memory T cells in the skin mediate durable immunity to melanoma. *Sci Immunol* 2017;2:eaam6346.
28 Molodtsov AK, Khatwani N, Vella JL, *et al*. Resident memory $CD8^+$ T cells in regional lymph nodes mediate immunity to metastatic melanoma. *Immunity* 2021;54:2117–32.
29 Zhang P, Côté AL, de Vries VC, *et al*. Induction of Postsurgical Tumor Immunity and T-Cell Memory by a Poorly Immunogenic Tumor. *Cancer Res* 2007;67:6468–76.
30 Im SJ, Hashimoto M, Gerner MY, *et al*. Defining CD8+ T cells that provide the proliferative burst after PD-1 therapy. *Nature New Biol* 2016;537:417–21.
31 Moran AE, Holzapfel KL, Xing Y, *et al*. T cell receptor signal strength in Treg and iNKT cell development demonstrated by a novel fluorescent reporter mouse. *J Exp Med* 2011;208:1279–89.
32 Andreatta M, Corria-Osorio J, Müller S, *et al*. Interpretation of T cell states from single-cell transcriptomics data using reference atlases. *Nat Commun* 2021;12:2965.
33 Mackay LK, Wynne-Jones E, Freestone D, *et al*. T-box Transcription Factors Combine with the Cytokines TGF-β and IL-15 to Control Tissue-Resident Memory T Cell Fate. *Immunity* 2015;43:1101–11.
34 Owen DL, Mahmud SA, Vang KB, *et al*. Identification of Cellular Sources of IL-2 Needed for Regulatory T Cell Development and Homeostasis. *J Immunol* 2018;200:3926–33.
35 Kim JM, Rasmussen JP, Rudensky AY. Regulatory T cells prevent catastrophic autoimmunity throughout the lifespan of mice. *Nat Immunol* 2007;8:191–7.
36 McLellan AD, Kapp M, Eggert A, *et al*. Anatomic location and T-cell stimulatory functions of mouse dendritic cell subsets defined by CD4 and CD8 expression. *Blood* 2002;99:2084–93.
37 Spitzer MH, Carmi Y, Reticker-Flynn NE, *et al*. Systemic Immunity Is Required for Effective Cancer Immunotherapy. *Cell* 2017;168:487–502.
38 Selby MJ, Engelhardt JJ, Quigley M, *et al*. Anti-CTLA-4 antibodies of IgG2a isotype enhance antitumor activity through reduction of intratumoral regulatory T cells. *Cancer Immunol Res* 2013;1:32–42.
39 Lee J, Ahn E, Kissick HT, *et al*. Reinvigorating Exhausted T Cells by Blockade of the PD-1 Pathway. *For Immunopathol Dis Therap* 2015;6:7–17.
40 Jansen CS, Prokhnevska N, Master VA, *et al*. An intra-tumoral niche maintains and differentiates stem-like CD8 T cells. *Nature New Biol* 2019;576:465–70.
41 Siddiqui I, Schaeuble K, Chennupati V, *et al*. Intratumoral Tcf1+PD-1+CD8+ T Cells with Stem-like Properties Promote Tumor Control in Response to Vaccination and Checkpoint Blockade Immunotherapy. *Immunity* 2019;50:195–211.
42 Connolly KA, Kuchroo M, Venkat A, *et al*. A reservoir of stem-like $CD8^+$ T cells in the tumor-draining lymph node preserves the ongoing antitumor immune response. *Sci Immunol* 2021;6:eabg7836.
43 Rahim MK, Okholm TLH, Jones KB, *et al*. Dynamic $CD8^+$ T cell responses to cancer immunotherapy in human regional lymph nodes are disrupted in metastatic lymph nodes. *Cell* 2023;186:1127–43.
44 Wing K, Onishi Y, Prieto-Martin P, *et al*. CTLA-4 control over Foxp3+ regulatory T cell function. *Science* 2008;322:271–5.
45 Ferris ST, Durai V, Wu R, *et al*. cDC1 prime and are licensed by $CD4^+$ T cells to induce anti-tumour immunity. *Nat New Biol* 2020;584:624–9.
46 Muranski P, Boni A, Antony PA, *et al*. Tumor-specific Th17-polarized cells eradicate large established melanoma. *Blood* 2008;112:362–73.
47 Franken A, Bila M, Mechels A, *et al*. $CD4^+$ T cell activation distinguishes response to anti-PD-L1+anti-CTLA4 therapy from anti-PD-L1 monotherapy. *Immunity* 2024;57:541–58.
48 Wei SC, Levine JH, Cogdill AP, *et al*. Distinct Cellular Mechanisms Underlie Anti-CTLA-4 and Anti-PD-1 Checkpoint Blockade. *Cell* 2017;170:1120–33.
49 Oliveira G, Stromhaug K, Cieri N, *et al*. Landscape of helper and regulatory antitumour CD4+ T cells in melanoma. *Nature New Biol* 2022;605:532–8.
50 Searles TG, Turk MJ. GSE279018. 2024. Available: https://www.ncbi.nlm.nih.gov/geo/
51 Stuart T, Butler A, Hoffman P, *et al*. Comprehensive Integration of Single-Cell Data. *Cell* 2019;177:1888–902.